Two new roles for the *Drosophila* AP patterning system in early morphogenesis

J. Todd Blankenship and Eric Wieschaus*

Howard Hughes Medical Institute, Department of Molecular Biology, Princeton University, Princeton, NJ 08544, USA

*Author for correspondence (e-mail: ewieschaus@molbio.princeton.edu)

SUMMARY

Although gastrulation is regarded as the stage during *Drosophila* development when the AP patterning system first influences morphological processes, transcription is regulated in complex patterns already at cycle 10. How soon this transcriptional complexity produces spatial differences in morphology has been unclear. We report on two new processes that establish visible morphological inhomogeneities before the onset of gastrulation. The first of these is the regulation of syncytial nuclear densities in the anterior end of the egg and represents the first zygotically driven AP asymmetry in the embryo. The second process is the generation of a fine-scale pattern in the actin/myosin array during cellularization. We find three domains of different yolk stalk diameters as well as depths of cellularization along the AP axis. These domains are established under the control of the AP patterning system and require *bicoid* activity. The anterior-most domain is a region of large yolk stalk diameters and corresponds to the region of decreased nuclear densities observed during syncytial stages. The middle domain shows smaller yolk stalk diameters and more rapid cellularization. Its establishment requires wild-type *paired* activity and thus indirectly requires *bicoid*. It occurs in a region of the embryo that ultimately gives rise to the cephalic furrow and may account for the effect of *paired* on that structure during gastrulation. Our results therefore suggest a link between cytoskeletal organization during cellularization and subsequent morphogenetic processes of gastrulation.

Key words: Gastrulation, Cellularization, *bicoid*, *paired*, Midblastula transition, *Drosophila*

INTRODUCTION

During embryonic development, spatial patterns commonly arise in a sequence of discrete steps. In *Drosophila*, the anterior-posterior (AP) patterning system establishes fine-scale pattern through a cascade of transcriptional regulation, beginning with maternally active coordinate genes, through gap genes and pair-rule genes, finally achieving cell by cell resolution at the level of the segment polarity genes (Pankratz and Jäckle, 1993). These changes in transcriptional activity occur concomitantly with a series of morphological transitions. The embryo begins its development as a syncytium of dividing nuclei (Foe et al., 1993). By the tenth nuclear division, all nuclei, with the exception of the yolk nuclei, have migrated to the periphery of the embryo. It is also during this tenth nuclear cycle that zygotic transcription begins. In cycle 14, the initial pattern of pair-rule gene activities is established and the embryo begins a process of cellularization. Each cortical nucleus is packaged in its own individual plasma membrane, thus forming a monolayered epithelium that sits upon a yolk sack (Schejter and Wieschaus, 1993a). Cellularization is the first morphological process reported to require a major input from the genome of the embryo. Injection of transcriptional inhibitors like α-amanitin blocks cellularization and causes a defect in the clearing of lipid droplets from the periphery of the embryo (Arking and Parente, 1980; Schubiger and Edgar, 1994; Merrill et al., 1988). During cellularization, the invaginating membrane front forms a widened canal held together apically by a basal adherens junction (Fullilove and Jacobson, 1971; Hunter and Wieschaus, 2000). The width of this 'furrow canal' increases as cellularization proceeds, eventually separating the blastoderm cells from the underlying yolk sack. The connections between the forming cells and the yolk sack ['yolk stalks' (Rickoll, 1976)] narrow as the furrow canal widens; a myosin driven contraction of the stalk may drive the widening of the canal. As the process of cellularization is finishing, pair-rule genes are expressed with single cell resolution and the first movements of gastrulation begin. In the cephalic furrow region, the first sign of gastrulation is a rapid cell shape change in which a row of cells, termed the initiator cells, shorten dramatically along their apical-basal axis and widen laterally. These movements begin while connections between the yolk and the cytoplasm of the cell still exist.

These seemingly discrete stages of development use common cytoskeletal components that must be adapted to serve new functions as the morphology of the embryo changes. For example, during the syncytial stages, nuclei are associated with broad caps of actin, separated by regions enriched in myosin, which are transformed into pseudocleavage furrows

during mitosis (Foe et al., 2000). The function of these caps is unknown, but they may be required for the proper spacing of nuclei in the syncytium (Postner et al., 1992). After the embryo enters cycle 14, the actin/myosin cytoskeleton is reorganized to allow cellularization. Myosin and actin now localize to the furrow canal where they contribute to the constriction of the stalks and may provide the force that drives membrane into the interior. The changing pattern in the cytoskeleton means that properties imparted by previous morphological events may set up constraints for subsequent stages of development. We report that, indeed, regulation in the spacing of syncytial nuclei affects properties of the actin/myosin array that forms during cellularization, and that regulation of the diameter of the actin/myosin array during cellularization may, in turn, affect the ability of gastrulation movements to occur.

We present two new morphogenetic processes that generate AP asymmetries long before those observed at gastrulation. We find that the first AP asymmetries driven by the genome of the embryo are visible by cycle 11, indicating that the complex patterns of gene expression during syncytial stages influence morphogenetic movements of these stages. We also argue that regulation by *bicoid* of the diameters of actin caps during syncytial cycles generates an anterior domain of lower nuclear densities. Second, we find that a new domain of faster cellularization occurs at the same position of the embryo as where the CF will eventually form. We suggest that this domain provides a link between cellularization and gastrulation in the requirement for the early expression of *paired* (*prd*), which appears to affect both the contractility of the cellularization apparatus and the initiation of the cephalic furrow at gastrulation.

MATERIALS AND METHODS

Fly strains

OregonR stocks were used as the wild-type strain in these experiments. The following mutant alleles were used in our analyses: bcd^{E1}, nos^{L7}, tsl^{146}, prd^4, prd^7, $eve^{1.27}$, eve^{R13}. BB5+18/FM7 stock was used to collect females carrying six copies of *bcd* (Driever and Nüsslein-Volhard, 1988). The fly strain carrying the histon2A-GFP fusion protein is described elsewhere (Clarkson and Saint, 1999).

Histology

Rabbit anti-Myosin (a generous gift from C. Field) was used to visualize yolk stalks, and mouse anti-neurotactin (BP106 from Developmental Studies Hybridoma Bank) was used as a marker of the basolateral surfaces of cells. Rabbit and guinea-pig anti-Eve (Rabbit anti-Eve originally generated by M. Frasch) as well as guinea pig anti-Prd were kindly given by J. Reinitz. Rabbit anti-Prd was a generous gift from C. Desplan. Oli-green (Molecular Probes) and Hoechst (Molecular Probes) were used to visualize nuclei. All the above reagents were used on heat fixed embryos following the protocol of Peiffer et al. (Peiffer et al., 1994). Secondary antibodies against rabbit and guinea pig IgG and conjugated to Alexa-488, Alexa-546, Alexa-568 and biotin were from Molecular Probes. Streptavidin-Cy5 was used to visualize biotinylated secondaries. Actin was visualized with Alexa-568-conjugated phalloidin (Molecular Probes) on embryos that were hand de-vitellinized after fixing for 45 minutes in heptane/18.5% formaldehyde-phosphate-buffered saline (PBS). Injected embryos were also hand de-vitellinized though the same process. Embryos were mounted in Aqua-Polymount (Polysciences) and examined on a Zeiss LSM 510 confocal microscope. Images were analyzed, processed and assembled with Adobe Photoshop 5.0.

α-amanitin injection

To block RNA transcription by RNA Pol II, a 100 μg/ml solution of α-amanitin (Sigma) was injected into dechorionated (Clorox bleach) and partially dessicated embryos. In the absence of lipid droplet clearing, which requires zygotic transcription, a golden haze of uncleared lipid droplet sits in the periphery of the embryo. Efficacy of injection was judged by this halo formation during lipid clearing.

Scanning electron microscopy

Embryos were dechorionated, fixed in formaldehyde (heptane/15% formaldehyde PBS), and de-vitellinized with methanol. They were then post-fixed in 4% osmium tetraoxide, dehydrated in an ethanol series and washed into a 100% tetramethylsilane (Ted Pella) solution that was allowed to sublimate away overnight. Embryos were mounted on aluminum tape on an aluminum stud and sputter coated with a gold-palladium mixture for 80 seconds. Images were taken on a Philips XL FEG-SEM scope.

Statistical analysis

Means and standard deviations were calculated using Microsoft Excel. Probabilities for the role of *prd* in the pre-CF domain were calculated using the rank-ordering system of a Mann-Whitney test for non-normal distributions. Probabilities for actin cap data were calculated using the Student's *t*-test. Measurements of actin caps were made with help of NIH Image v1.62, and then data pasted into Microsoft Excel and analyzed.
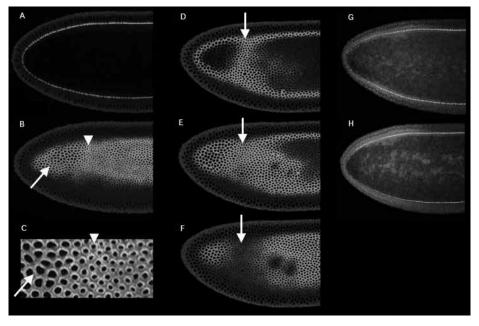
RESULTS

Three domains of varying yolk stalk diameter and depth of cellularization along the AP axis

To assay the degree of uniformity along the AP axis during cellularization, we visualized the furrow canals of wild-type embryos by staining for Myosin. We found that by mid-cellularization, three domains of differing diameters of yolk stalks could be observed. The first domain is centered around the anterior pole of the embryo, and possesses the largest diameters (arrow in Fig. 1B,C). The second domain, immediately posterior to the first anterior domain, has the smallest diameters (arrowhead in Fig. 1B,C). This domain is centered around the location of where the cephalic furrow will eventually form. The third domain lies posterior to this pre-CF domain and has furrow canals of intermediate diameter (Fig. 1B,C).

These three domains also differ in the depth of the cellularization front. The anterior domain, which has large yolk stalk diameters, is the shallowest part of the embryo in its depth of cellularization (Fig. 1G,H). By the end of cellularization, the most anterior part of this domain can possess a depth of cellularization (15-20 μm) half that of the rest of the embryo (~35 μm on average). The region posterior to the pre-CF domain has an intermediate depth (Fig. 1D-H), whereas the pre-CF domain, which has the smallest yolk stalk diameters, has the greatest depth of cellularization (arrow in Fig. 1D-F). The easiest way to visualize the greater depth of the pre-CF domain is by using the optical sectioning of the confocal microscope. By taking thin, 1 μm sections, we see a difference of 2-3 μm between the base of the pre-CF domain (Fig. 1D) and the base of cells in the rest of the embryo (Fig. 1F). Thus, the regions of differing yolk stalk diameters correspond to the regions of varying depth during cellularization.

Fig. 1. Three domains of yolk-stalk diameters and depth of cellularization. Wild-type embryos stained for Myosin. (A) Cross-section of late-cellularization embryo showing depth of cellularization. (B) Same embryo as in A observed in grazing section at the depth of the furrow canals. (C) Higher magnification view of B. Arrows in B,C indicate anterior domain, arrowheads indicate pre-CF domain. (D-F) 1 μm optical sections of wild-type embryo proceeding from interior of embryo (D) towards surface-most section (F). Each section is separated from the next by 2 μm. Arrows indicate pre-CF domain. (G,H) +/CyO, hb-*lacZ* embryo stained for Myosin (basal localization, same as in A) and β-gal (cytoplasmic). These embryos are normal for cellularization, but the cytoplasmic β-gal allows for easier visualization of cell depth. The great difference in the depth of cellularization between the anterior pole (~15-20 μm) and the rest of the embryo (~35 μm) means that this difference can be seen in a cross-sectional view of the embryo. The small difference in depth between the pre-CF domain and the posterior domain (a difference of 2-3 μm) means that this difference can not be easily viewed in cross-section (G,H), but can be visualized with optical sectioning technique (D-F).

The AP patterning system regulates the cellularization domains

To test whether these cellularization phenomena are due simply to the position or geometry of the embryo (e.g. the curvature of the anterior part of the egg), or if these phenomena are being specified and positioned by the AP patterning system, we looked for the three domains in embryos that lacked all positional information along this axis. In embryos derived from females triply mutant for *bicoid nanos torso-like*, yolk stalk diameters are uniform, even though other aspects of cellularization occur normally (Fig. 2B,C). The shallow cellularization front of the anterior domain (Fig. 2F,G), as well as the greater depth of the pre-CF, is also lost (Fig. 2B,C). Thus, these phenomena require the activity of the AP patterning system for their morphogenesis.

These cellularization phenomena respond to specific levels of the *bicoid* gradient. Embryos that carry six copies of *bicoid* produce more Bicoid protein, shifting any given concentration of Bicoid to a position posterior to where it would be in a wild-type embryo. In embryos carrying six copies of *bicoid*, the pre-CF domain of small yolk stalk diameters and greater depth is shifted posteriorly, while the anterior domain of large yolk stalk diameters expands to cover close to half of the embryo (Fig. 2D,E). *bicoid* appears to be the important factor specifying these phenomena, as embryos derived from females mutant for *bicoid* lack the anterior and pre-CF domains (data not shown).
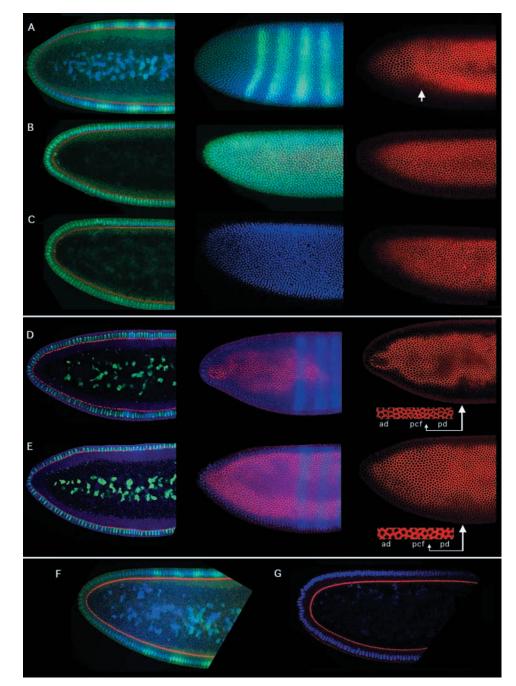
A pair-rule gene, *prd*, specifies the pre-CF domain

Since the pre-CF domain is a relatively narrow domain, it seemed unlikely that the broad Bicoid gradient would be directly specifying the pre-CF domain. Several pair-rule genes are expressed in approximately the right time and place to be mediating the formation of the pre-CF domain. While Even-skipped (Eve) is expressed in the posterior half of the pre-CF

domain (data not shown), Prd expression is directly centered on the pre-CF domain (Fig. 3C-E). Prd expression also has an unusual feature. When Prd expression is first detected during cycle 13, it is observed in a single, gap gene-like domain (Fig. 3A,B). Thus, Prd is expressed before the pre-CF domain is formed, and in the right location in the embryo. Moreover, the early expression of Prd in a single stripe, rather than in the stereotypical seven-stripe pattern, suggests that it could specify the pre-CF domain independent of other factors.

We then analyzed various patterning mutants for a disruption of the pre-CF domain. *prd* homozygotes show a normal anterior domain of larger yolks (ad in Fig. 3G), but there is very little difference in the yolk stalk diameters between the pre-CF domain and the posterior domain (compare pcf and pd diameters in Fig. 3G). The relatively subtle appearance of the pre-CF domain in different genetic backgrounds required the scoring of embryos in a blind test. On a classification scale of 0-5, with 0 indicating a complete absence of the pre-CF domain, *prd* homozygotes scored a 1.2, while their non-homozygous siblings scored a 3.3. A Mann-Whitney ranked sum test indicates that these classifications are significant ($P \ll 0.001$, $n=61$). Representative examples of the pre-CF domain in *prd*/+ (Fig. 3F) and *prd*⁻ (Fig. 3G) are shown in Fig. 3. Thus, *prd* is already active in the regulation of morphogenesis during the process of cellularization.

An anterior domain of lower nuclear densities pre-figures the cellularization network

The pre-CF domain is first visible when the cellularization front has reached about 25% of its depth. However, the larger yolk stalks of the anterior domain are visible throughout cellularization. We find that the density of nuclei in the anterior is reduced by about 30% from the nuclear density that is found in the rest of the embryo. This anterior domain of lower nuclear density is centered around the anterior pole and extends to

Fig. 2. The AP patterning system specifies the spatial pattern of cellularization. (A) An embryo from a *bcd nos tsl*/+ female. (B,C) Embryos from *bcd nos tsl* homozygous females. (A-C) First column: cross section through embryo showing stage of cellularization. Second column: focal plane through nuclei showing slightly anterior shift of Eve stripes (A), ubiquitous Eve (B), and minus the green channel (C) for better resolution of nuclei. Third column: focal plane through furrow canals showing uniform stalk diameters in (B,C). Red, Myosin; Green, Eve; Blue, DNA (Hoechst). The arrow marks the position of the first stripe of Eve in embryos in which the green channel has been removed so that yolk stalks may be seen more easily. Embryos from D,E are derived from females carrying six copies of *bicoid*. (D-E) First column: cross section through embryo showing stage of cellularization. Second and third columns: two different focal planes of furrow canals. Red, Myosin; Green, DNA; Blue, Eve. The embryos in the third column of D,E have had the blue channel removed so the yolk stalks can be clearly seen. The thin strips in the third row are higher magnifications of yolk stalks from the anterior domain (ad), pre-CF domain (pcf) and posterior domain (pd). (F,G) Cross sections through embryos showing stage of cellularization and depth of cellularization front. (F) Embryo from *bcd nos tsl*/+ female; (G) a *bcd nos tsl* homozygous female. Note deeper extent of cellularization front in the anterior in G than in the anterior in F.

approximately two to three nuclei in front of the first stripe of Eve, or ~70% EL (see Fig. 5, cycle 14 embryo; Fig. 7A). Judging from the staining patterns of Eve and Prd, this is the same area of the embryo in which the anterior domain of large yolk stalk diameters meets the pre-CF domain. During cellularization the anterior nuclear domain is consistently observed in OreR embryos with an average decrease in nuclear density of 27.6% (*n*=42, s.d.=4.4%). In this sample, the values for individual embryos ranged from 34% to 20%. This domain of lower nuclear densities is maintained and stays constant throughout the process of cellularization (Fig. 4A,B), and can still be observed in gastrulating embryos (Fig. 5). This greater spacing of nuclei in the anterior would necessarily lead to a

cellularization network with larger diameters. Additionally, by mid-cellularization, when a pre-CF domain is already visible, a slight clustering of nuclei in this region occurs (arrow in Fig. 4B).

As the anterior domain of lower nuclear densities is present at the start of cycle 14, we asked when this AP asymmetry arises. While the sphere of nuclei that migrate to the surface of the embryo during cycle 9, and the cortical nuclei of cycle 10 are uniform along the AP axis, the first sign of increased nuclear spacing in the anterior can be observed in cycle 11 embryos. By cycle 12, a pronounced AP asymmetry is observed, which is maintained through the subsequent mitosis to the start of cellularization (Fig. 5, fixed 6 × *bcd* embryo (for
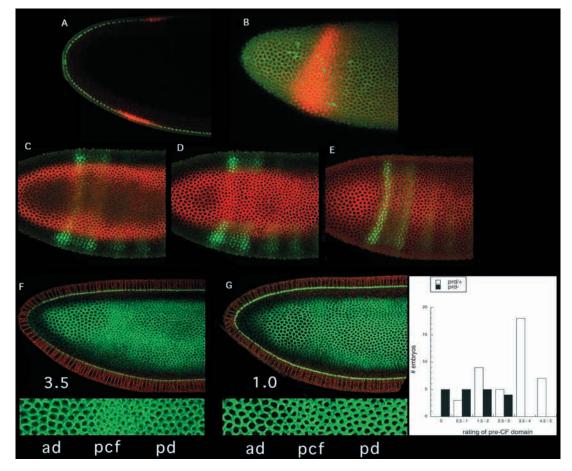
Fig. 3. Prd expression overlaps with the pre-CF domain and *paired* is required for the pre-CF domain to form. Cross-section (A) and surface view (B) through a very early cycle 14 embryo showing Myosin (green) and the early single stripe expression of Prd (red). Optical sections from basal side of yolk stalks (C), through yolk stalks (D) and apical side of yolk stalks (E) showing overlap of first stripe of Prd expression (green) with pre-CF domain (deeper band of cellularization front as marked by Myosin in red). A lateral part of embryo (D) has had the green channel removed so the smaller yolk stalks of the pre-CF domain can be seen. (F,G) Representative example of prd/+ embryo (F, classified as 3.5 on 0-5 scale), and its homozygous *prd* sibling (G, classification of 1.0) stained with Myosin (green) and Neurotactin (a general cell surface marker in red). Embryos were also stained against Prd in far-red channel for genotyping purposes (not shown). (F,G) Embryos are a composite of a cross-section focal plane with the furrow canal focal plane super-imposed. The thin strips in the third row are higher magnifications of yolk stalks from the anterior domain (ad), pre-CF domain (pcf) and posterior domain (pd). The remaining inhomogeneity in the region of the pre-CF domain in G may reflect the role of additional AP patterning genes in the specification of this domain. The graph shows the results of a blind scoring of the pre-CF domain in *prd/+* and *prd⁻* homozygous embryos. The data illustrates that although a minority of *prd* heterozygotes possess a poor pre-CF domain, no *prd⁻* homozygotes form a normal pre-CF domain (a rating of 3.5 or higher).
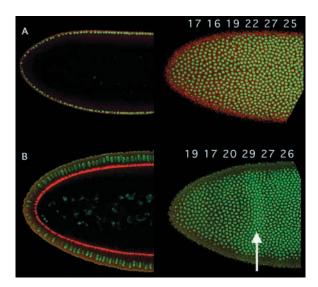
reasons stated in figure legend) on left, GFP-histone time-lapse series on right). The anterior domain of lower nuclear densities is also observable in living embryos. Nuclear counts on GFP-histone embryos demonstrates a similar ~30% reduction in nuclear density in vivo (Fig. 5, movies from three different embryos showed 30%, 29% and 26% differences in density at cycle 14). These observations on living embryos also reveals that, except for when the nuclei are undergoing mitosis and the associated yolk contractions, the anterior nuclear domain is present throughout the rest of the cell cycle.

Before cycle 14, cortical nuclei are associated with large actin caps. In embryos without actin caps, the regular spacing of nuclei is disrupted (Postner et al., 1992). One possible mechanism for the formation of the anterior domain of lower nuclear densities would use the regulation of the size of these actin caps. To see if asymmetries in actin cap size occur along the AP axis, we stained wild-type embryos with fluorescently labeled phalloidin to visualize F-actin. Measurements showed that anterior actin caps were larger than caps in the rest of the embryo in cycle 11 and cycle 12, but not during cycle 10 (Fig. 6, Table 1). This difference, although small, is highly reproducible from embryo to embryo. In cycle 11, the values for six different embryos were 8%, 7%, 8%, 6%, 7% and 9%.

The AP patterning system specifies the anterior domain of lower nuclear density through zygotic transcription

The exceptionally early appearance of the AP asymmetries in nuclear distributions led us to examine whether the anterior domain of lower nuclear densities is specified by the AP patterning system. In embryos derived from *bicoid nanos torso-like* mutant females, nuclear spacing is uniform along the

Fig. 4. An anterior domain of lower nuclear densities is formed before the start of cellularization. Embryos are stained against Myosin (red) and DNA (green). First column: cross-section showing absence of cellularization front. Second column: focal plane though nuclei. Numbers across the top represent nuclei counts in a square of constant size (70×70 pixel box) positioned at corresponding points along the AP axis of the embryo. (A) A pre-cellularization, cycle 14 wild-type embryo shows a lower density of nuclei in the anterior. (B) A late-stage cellularizing embryo shows a similar anterior nuclear density as in A, but also has an additional slight clustering of nuclei in the region of the pre-CF domain (arrow).

AP axis (Fig. 7B). In addition, the anterior nuclear domain can be expanded posteriorly in embryos carrying six copies of *bicoid* (Fig. 7C). Additionally, embryos from *bicoid* females are uniform in their nuclear densities (data not shown), arguing that the anterior domain of lower nuclear densities is set up by the Bicoid gradient. Finally, the larger diameters of the actin caps in the anterior do not occur in embryos from *bicoid nanos torso-like* females (Fig. 6, Table 1).

As zygotic transcription only starts around cycle 10, the early appearance of the anterior domain by cycle 11 raised the question of whether zygotic transcription is required for its formation. It is possible that *bicoid* might be regulating nuclear spacing through a post-transcriptional mechanism (Chan and Struhl, 1997). To assay the effect of transcription on nuclear spacing, we injected embryos with α-amanitin to block RNA polymerase II. Consistent with earlier studies, such embryos develop to cycle 14 with normal gross morphology. However, when we examine these embryos with nuclear stains, they show a total absence of asymmetric nuclear distributions. Embryos injected with α-amanitin fail to form the anterior domain of lower nuclear densities (less than 5% difference between nuclear density from the anterior to the posterior, n=18, also Fig. 7E,F), but all control embryos injected with water continued to show an anterior domain (greater than 20%
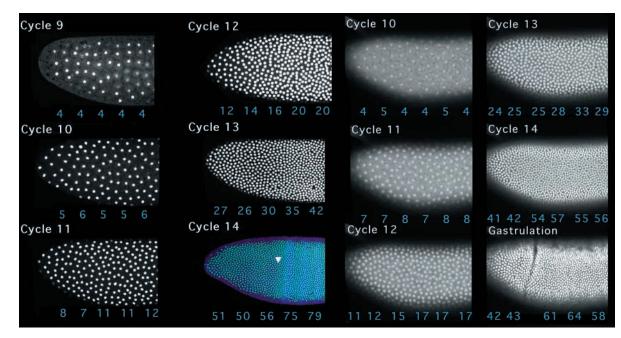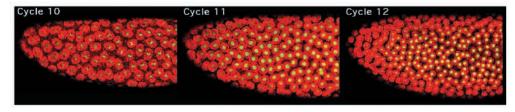

Fig. 5. Left-hand six pictures: the anterior domain of lower nuclear densities arises by cycle 11. To facilitate visualization of the anterior domain, and to reduce the impact of the complicating geometry of the curvature at the anterior pole, embryos with a larger anterior domain (from females carrying six copies of *bicoid*) were scored for the distribution of nuclei (marked by oli-green). Similar results were obtained from the nuclear counts of wild-type embryos (GFP-histone embryo, and data not shown). The numbers represent nuclei counts in a square of constant size (70×70 pixel box) positioned at corresponding points along the AP axis of the embryo. The final image in the fixed embryos series shows Eve stripes (blue). The arrowhead marks the position of the border of the anterior domain, several nuclei to the anterior of the first stripe of Eve. The right-hand six pictures are a time-lapse series of a single embryo carrying a GFP-histone transgene. Owing to differences in magnification from using two different microscopes to capture the images, the same size square yields different densities between the fixed embryo series and the live embryo series, as well as in Fig. 4. Note that the relative difference between the anterior domain and the rest of the embryo is similar. The position of the CF can be seen in the final image of the GFP-histone embryo (gastrulation), and this position can be used as reference point for the AP axis in the other embryos as the same focal plane was kept at all time points.

Fig. 6. Actin caps in the anterior domain possess larger actin caps than in the rest of the embryo. Actin caps in cycle 10, cycle 11 and cycle 12 wild-type embryos were visualized by Alexa-568 phalloidin (red). Nuclei (DNA marked by oli-green) are in green.

difference in nuclear density, n=15, also Fig. 7D). We conclude that *bicoid* regulates the zygotic transcription to bring about the formation of the anterior domain of lower nuclear densities.

A delay in cephalic furrow formation in *prd* embryos

Our previous work has identified two genes necessary for cephalic furrow formation. Embryos mutant for either *eve* or *buttonhead* (*btd*) lacked cephalic furrows (Fig. 8E,F). Further work indicated that both *eve* and *btd* have a defect in the earliest phase of CF formation, which is initiator cell formation. At no point during development are the stereotypical cell shape changes of shortening along the apical-basal axis and widening of the cell observed in these mutants. Mutations in *prd* also cause a disruption in CF formation. At the onset of gastrulation, the cephalic furrow does not form, nor do initiator cells undergo their characteristic cell shape change (Fig. 8H). Because there is an absolute correlation between initiator cell behavior and the middle nucleus of the first stripe of Eve in wild-type embryos (Vincent et al., 1997), the location where initiator cells should form in *prd* embryos can still be identified. In *prd* embryos these Eve-marked cells are indistinguishable from their neighbors at stages during gastrulation when the ventral furrow has formed and the CF would normally be visible in wild-type embryos (Fig. 8G,H). However, by mid-germband extension (GBE), *prd* embryos have formed a regular, CF-like invagination (Fig. 8D). We believe that this late fold arises through the same mechanisms that govern normal CF formation, but that these processes are delayed relative to the development of wild-type embryos (in the stage 7 *prd* embryo (Fig. 8B), there are no cell shape changes in the region where the CF would form, while the

stage 6 wild-type embryo (Fig. 8A) has an obvious CF. Initiator cells form in wild-type embryos at stage 6, at the onset of gastrulation (arrows in Fig. 8G). Imaging of *prd* embryos reveals initiator cell activities beginning at stage 7 (arrows in Fig. 8J). At this stage, wild-type embryos have already begun to deform the yolk sack with a basal bulge of the epithelium (Fig. 8I). At the beginning of stage 8, or germband extension, wild-type embryos have a furrow that is many cells deep (Fig. 8K), while *prd* embryos have just begun to deform the yolk sack (Fig. 8L). It is only by mid-GBE that most, but not all, *prd* embryos have a regular CF stretching around the entire circumference of the embryo.

DISCUSSION

A link between cellularization and gastrulation

The abnormalities in CF formation observed at the beginning of gastrulation in *prd* embryos are superficially similar to those observed in embryos mutant for *eve* or *btd*. In the absence of the activity of *eve*, *btd* or *prd*, the cell shape changes that occur in the row of cells that initiate CF formation at the beginning of gastrulation do not occur. In contrast to *eve* or *btd*, however, we have identified early activities of *prd* during cellularization that may account for the later differences observed in CF formation. Consistent with this view our analysis indicates that *prd* embryos often recover and form a fairly regular CF by mid-germband extension, unlike the severe disruption of the CF in *eve* and *btd* embryos (Fig. 8) (Vincent et al., 1997). Sander et al. (Sander et al., 1980), who discovered the original *prd* allele, noted that 'gastrulation seemed delayed and that the cephalic

Table 1. Measurements of the diameters of actin caps in the region of the anterior domain and posterior to the anterior domain

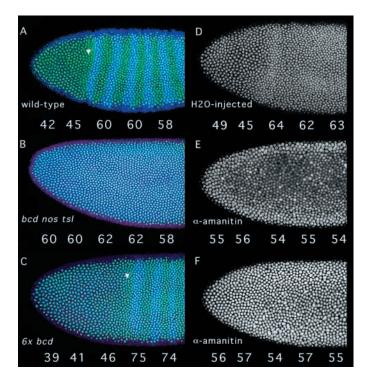|	Anterior mean (s.d.)	Posterior mean (s.d.)	Percent difference between A/P (positive value indicates larger anterior caps)	Caps measured	Probability of significance
Wild type					
Cycle 10	19.2 μm (2.28)	19.5 μm (2.26)	−1.54%	260	Not significant (*P*=0.290)
Cycle 11	15.5 μm (1.84)	14.3 μm (1.87)	8.39%	418	Significant (*P*<0.001)
Cycle 12	9.61 μm (1.53)	9.06 μm (1.00)	6.07%	193	Significant (*P*=0.003)
bcd nos tsl					
Cycle 10	17.8 μm (2.48)	17.2 μm (2.45)	3.30%	152	Not significant (*P*=0.174)
Cycle 11	13.6 μm (1.86)	13.7 μm (1.85)	−1.38%	401	Not significant (*P*=0.328)
Cycle 12	10.4 μm (0.898)	10.7 μm (1.23)	−2.90%	166	Not signficant (*P*=0.080)

1588 caps were measured.

Fig. 7. The AP patterning system regulates the anterior domain of lower nuclear densities through transcription. (A) Wild-type embryo with anterior lower nuclear density. (B) Embryo from *bcd nos tsl* female with uniform nuclear density. (C) Embryo from female carrying six copies of *bicoid* showing expanded domain of lower nuclear densities. Arrowheads in A,C indicate the approximate border of the anterior domain. (D) Control wild-type embryo injected with water exhibiting an anterior domain. (E,F) Wild-type embryos injected with α-amanitin demonstrating uniform nuclear densities. The images are a focal plane through nuclei (green, as marked by DNA stain), and stained against Eve (blue in A-C). Note the uniform Eve in embryo from *bcd nos tsl* female (B) and the posterior shift in the Eve stripes in embryo from female carrying six copies of *bicoid* (C).

furrow either fails to appear or forms some time after the onset of germband extension'. Our work refines and extends their observations. While the start of gastrulation occurs normally in *prd* embryos, CF formation and initiator cell behavior is delayed. We propose that this delay is due not to a function of *prd* during gastrulation in the specification of initiator cells, as we have proposed for *eve* and *btd* function. These latter mutants completely block initiator cell and CF formation. Instead, we show that *prd* function is necessary for the formation of the pre-CF domain, and suggest that it is only through this disruption of the pre-CF domain that *prd* functions in CF formation. The recovery of the CF observed in *prd* embryos may be a reflection that cellularization throughout the embryo has finally reached the point that the pre-CF domain reaches at the very beginning of gastrulation, and so CF formation, although delayed, may be correctly initiated. The advanced rate of cellularization in the pre-CF domain may reflect a required premature closing of the base of the initiator cells so that cell volumes may be maintained during the severe cell shape changes of gastrulation, or that cytoskeletal components involved in cellularization must be freed for initiator cell movements. Because little deformation, or loss of

volume, occurs in the presumptive initiator cells of early *prd* embryos (arrows in Fig. 8H), we favor the latter of these two possibilities. Thus, the subtle regulation of one stage of development can have profound effects upon a later, seemingly discrete, process of development.

The generation of spatial pattern in the cellularization network

The cellularization front that arises during early cycle 14 is rich in actin and myosin, and is thought to provide a contractile force that orients and drives the process of cellularization (Warn et al., 1980; Warn and Magrath, 1983). This network, as well as cellularization itself, proceeds through a two-phase process. The first phase is a basal movement of the cellularization front towards the interior of the embryo. During this phase, the furrow canals stay constant in their small size, and the actin/myosin array has a hexagonal shape. The second phase is a lateral movement of the cellularization front, which creates a pinching off at the bases of cells in the newly forming cell sheet (Schejter and Wieschaus, 1993b). We have found that the morphology of the cellularization front is not uniform along the AP axis. The pre-CF domain is distinguished from other regions of the embryo by its small yolk stalk diameters and greater depth of cellularization.

Our results suggest the following model for the generation of AP asymmetries during cellularization. In the pre-CF domain, the Bicoid gradient directs the correct localization of the early gap gene-like expression domain of *prd*, which, in turn, directs a greater local contraction of the cellularization network. When cellularization is in its first phase of inward directed movement, the greater contraction of the pre-CF domain leads to a greater advance inwards of the cellularization front, thus creating the greater depth of the pre-CF domain. Then, when cellularization shifts to the second phase of a lateral, pinching-off movement, the greater contractility of the pre-CF domain leads to a greater widening of the furrow canals, which creates the smaller yolk stalk diameters observed in the pre-CF domain. The creation of this domain of advanced cellularization may be necessary for the initiator cell shape change required for cephalic furrow formation.

In certain respects, the anterior domain of large yolk stalk diameters and shallow cellularization appears to be the opposite of the pre-CF domain, and thus might be produced by a downregulation of the same contractile mechanisms that we propose operate in the pre-CF domain. However, we have found that the formation of the larger yolk stalk diameters in the anterior domain clearly involves a different mechanism. The anterior cellularization domain is pre-figured by an anterior domain of lower nuclear densities, while the pre-CF domain initiates in a region where nuclear densities are uniform. The greater spacing of nuclei in the anterior necessarily causes the formation of actin/myosin arrays of greater diameter during cellularization. We favor a model for the formation of the anterior domain in which the *bicoid* gradient, by cycle 11, has regulated the transcription of a set of zygotic genes, which in turn regulate the size of the actin caps overlaying the nuclei. This regulation of the actin caps results in larger caps in the anterior that necessitates a greater spacing of nuclei. By cycle 14, when cellularization is initiated, the greater spacing of nuclei dictates the generation of a cellularization network in the anterior in which the hexagonal
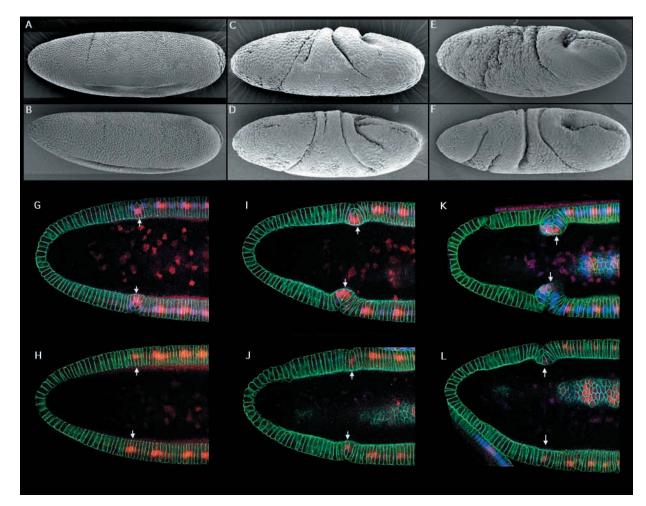
Fig. 8. *prd* embryos have a delay in initiator cell behavior and CF formation. (A-D) Scanning electron microscopy of wild-type (A,C), *prd* (B,D), *eve* (E) and *btd* (F) embryos. Embryos are viewed on their lateral sides and are at early gastrula (A,B) and at mid-germband extension (C-F). (G-L) Embryos are stained with neurotactin (green), Eve (red) and Prd (blue). *prd* homozygotes were identified based on the absence of Prd staining. *prd* (H,J,L) or non-*prd* sibling (G,I,K) embryos of similar stages of gastrulation are shown. (G,H) Embryos are at the very onset of gastrulation. (I,J) Approximately 15 minutes into gastrulation; (K,L) early germband extension. Prd is expressed in the cell immediately anterior to the initiator cell, which corresponds to the middle cell of the first stripe of Eve. Eve and Prd therefore overlap in a single cell. Arrows mark either the initiator cell or the cell that would be an initiator cell in a wild-type embryo, as marked by localization relative to Eve expression. Note that the embryo in L, although at early germband extension, has barely begun a basal bulge of the CF and only on one side.

components are larger in diameter. The initiation of a large hexagons would thus lead to larger yolk stalks. It may be that the larger hexagons of the cellularization network contract less efficiently, thus generating the shallower depth of cellularization that is observed for the anterior domain.

A *Drosophila* MBT?

The concept of a mid-blastula transition (MBT) has generally referred to a time when the genome of an embryo begins to exert an influence on development, presumably through zygotic transcription. The best-defined MBT is for *Xenopus* (Newport and Kirschner, 1982a; Newport and Kirschner, 1982b), where the MBT was characterized by a cessation of synchronous mitotic cycles, the start of zygotic transcription, and a change in the morphology of blastula cells (i.e., the acquisition of cell motility). Various aspects of this characterization have since been called into question. There is low level zygotic transcription before the MBT, and it appears

as though cell motility may not be a function of zygotic transcription, but of slower mitosis (Kimelman et al., 1987). Although these discrepancies call into question the usefulness of the MBT as a concept (Yasuda and Schubiger, 1992), the idea of an MBT remains an attractive model for explaining the changing morphology of the *Drosophila* embryo.

In flies, the MBT has traditionally been discussed in terms of cycle 14 development. It is at this point that the fly embryo ceases its synchronous syncytial divisions and several morphogenetic processes require zygotic transcription for their genesis. At a superficial level, the first observable defects in embryos deficient for zygotic transcription was at cycle 14, when α-amanitin-injected embryos showed defects in the processes of lipid droplet clearing and cellularization. However, as in *Xenopus*, defining a precise MBT has some difficulties. Although cycle 14 marks a major increase in transcriptional efficiency (Zalokar, 1976), the start of zygotic transcription occurs in different nuclear cycles for different

genes. In general, for the early acting genes involved in patterning, transcription begins around cycle 10, although some genes are transcribed as early as cycle 8 (Pritchard and Schubiger, 1996), and mutations in specific segmentation genes show subtle disruption as early as cycle 10 (Karr et al., 1985). What is striking in the results we report for Bicoid and Prd is the correspondence between spatial patterns of expression and regional alterations in morphology. Our results show that the genome of the embryo is active in the spatial regulation of morphogenesis at a much earlier time than previously described. The genome directs reproducible asymmetries in morphology by cycle 11. The generation of an anterior domain of lower nuclear densities argues against a single discrete MBT at cycle 14 (Yasuda and Schubiger, 1992). Our results further suggest a more refined view of the Drosophila MBT in which there is a gradual shifting in the guidance of development from maternal to zygotic gene products, one that stretches from as early as cycle 8 until the cessation of mitosis and formation of a cellularized embryo at cycle 14.

REFERENCES

Arking, R. and Parente, A. (1980). Effects of RNA inhibitors on the development of Drosophila embryos permeabilized by a new technique. *J. Exp. Zool.* **212**, 183-194.

Chan, S. K. and Struhl, G. (1997). Sequence-specific RNA binding by *bicoid*. *Nature* **388**, 634.

Clarkson, C. and Saint, R. (1999). A His2AvDGFP fusion gene rescues His2AvD mutant lethality and provides an *in vivo* marker for Drosophila chromosome behavior. *DNA Cell Biol.* **18**, 457-462.

Driever, W. and Nusslein-Volhard, C. (1988). The bicoid protein determines position in the Drosophila embryo in a concentration-dependent manner. *Cell* **54**, 95-104.

Foe, V. E., Odell, G. M. and Edgar, B. A. (1993). *The Development of* Drosophila melanogaster. Cold Spring Harbor, NY: Cold Spring Harbor Laboratory Press.

Foe, V. E., Field, C. M. and Odell, G. M. (2000). Microtubules and mitotic cycle phase modulate spatiotemporal distributions of F-actin and myosin II in Drosophila syncytial blastoderm embryos. *Development* **127**, 1767-1787.

Fullilove, S. L. and Jacobson, A. G. (1971). Nuclear elongation and cytokinesis in Drosophila montana. *Dev Biol.* **26**, 560-577.

Hunter, C. and Wieschaus, E. (2000). Regulated expression of nullo is required for the formation of distinct apical and basal adherens junctions in the Drosophila blastoderm. *J. Cell Biol.* **150**, 391-401.

Karr, T. L., Ali, Z., Drees, B. and Kornberg, T. (1985). The engrailed locus of D. melanogaster provides an essential zygotic function in precellular embryos. *Cell* **43**, 591-601.

Kimelman, D., Kirschner, M. and Scherson, T. (1987). The events of the midblastula transition in Xenopus are regulated by changes in the cell cycle. *Cell* **48**, 399-407.

Merrill, P. T., Sweeton, D. and Wieschaus, E. (1988). Requirements for autosomal gene activity during precellular stages of Drosophila melanogaster. *Development* **104**, 495-509.

Newport, J. and Kirschner, M. (1982a). A major developmental transition in early Xenopus embryos: I. characterization and timing of cellular changes at the midblastula stage. *Cell* **30**, 675-686.

Newport, J. and Kirschner, M. (1982b). A major developmental transition in early Xenopus embryos: II. Control of the onset of transcription. *Cell* **30**, 687-696.

Pankratz, M. J. and Jäckle, H. (1993). *The Development of* Drosophila melanogaster. Cold Spring Harbor, NY: Cold Spring Harbor Laboratory Press.

Peiffer, M., Sweeton, D., Casey, M. and Wieschaus, E. (1994). *wingless* signal and Zeste-white 3 kinase trigger opposing changes in the intracellular distribution of Armadillo. *Development* **120**, 369-380.

Postner, M. A., Miller, K. G. and Wieschaus, E. F. (1992) Maternal effect mutations of the sponge locus affect actin cytoskeletal rearrangements in Drosophila melanogaster embryos. *J. Cell Biol.* **119**, 1205-1218.

Pritchard, D. K. and Schubiger, G. (1996). Activation of transcription in Drosophila embryos is a gradual process mediated by the nucleocytoplasmic ratio. *Genes Dev.* **10**, 1131-1142.

Rickoll, W. L. (1976). Cytoplasmic continuity between embryonic cells and the primitive yolk sac during early gastrulation in Drosophila melanogaster. *Dev. Biol.* **49**, 304-310.

Sander, K., Lohs-Schardin, M. and Baumann, M. (1980). Embryogenesis in a Drosophila mutant expressing half the normal segment number. *Nature* **287**, 841-843.

Schejter, E. D. and Wieschaus, E. (1993a). Functional elements of the cytoskeleton in the early Drosophila embryo. *Annu. Rev. Cell Biol.* **9**, 67-99.

Schejter, E. D. and Wieschaus, E. (1993b). *bottleneck* acts as a regulator of the microfilament network governing cellularization of the Drosophila embryo. *Cell* **75**, 373-385.

Schubiger, G. and Edgar, B. (1994). Using inhibitors to study embryogenesis. *Methods Cell Biol.* **44**, 697-713.

Vincent, A., Blankenship, J. T. and Wieschaus, E. (1997). Integration of the head and trunk segmentation systems controls cephalic furrow formation in Drosophila. *Development* **124**, 3747-3754.

Warn, R. M., Bullard, B. and Magrath, R. (1980). Changes in the distribution of cortical myosin during the cellularization of the Drosophila embryo. *J. Embryol. Exp. Morphol.* **57**, 167-176.

Warn, R. M. and Magrath, R. (1983). F-actin distribution during the cellularization of the Drosophila embryo visualized with FL-phalloidin. *Exp. Cell Res.* **143**, 103-114.

Yasuda, G. K. and Schubiger, G. (1992). Temporal regulation in the early embryo: is MBT too good to be true? *Trends. Genet.* **8**, 124-127.

Zalokar, M. (1976). Autoradiographic study of protein and RNA formation during early development of Drosophila eggs. *Dev Biol.* **49**, 425-437.